THE JOURNAL OF PHYSICAL CHEMISTRY Letters

Letter

pubs.acs.org/JPCL

# Macrocrystals of Colloidal Quantum Dots in Anthracene: Exciton Transfer and Polarized Emission

Zeliha Soran-Erdem,[†,∥] Talha Erdem,[†,∥] Pedro Ludwig Hernandez-Martinez,[‡] Mehmet Zafer Akgul,[†] Nikolai Gaponik,[§] and Hilmi Volkan Demir*[,†,‡]

[†]Departments of Electrical and Electronics Engineering, Physics, UNAM−National Nanotechnology Research Center, and Institute of Materials Science and Nanotechnology, Bilkent University, Ankara 06800, Turkey

[‡]School of Electrical and Electronic Engineering and School of Physical and Mathematical Sciences, Nanyang Technological University, 639798, Singapore

[§]Physical Chemistry, TU Dresden, Bergstrasse 66b, D-01062 Dresden, Germany

Supporting Information

**ABSTRACT:** In this work, centimeter-scale macrocrystals of nonpolar colloidal quantum dots (QDs) incorporated into anthracene were grown for the first time. The exciton transfer from the anthracene host to acceptor QDs was systematically investigated, and anisotropic emission from the isotropic QDs in the anthracene macrocrystals was discovered. Results showed a decreasing photoluminescence lifetime of the donor anthracene, indicating a strengthening energy transfer with increasing QD concentration in the macrocrystals. With the anisotropy study, QDs inside the anthracene host acquired a polarization ratio of ∼1.5 at 0° collection angle, and this increases to ∼2.5 at the collection angle of 60°. A proof-of-concept application of these excitonic macrocrystals as tunable color converters on light-emitting diodes was also demonstrated.

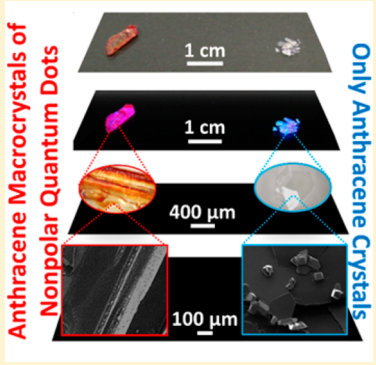


In recent years, colloidal nanocrystal quantum dots (QDs) have attracted significant attention in the field of photonics because they provide tunable and narrow-band emission spectra accompanied by broad absorption spectra, large quantum efficiency, and relatively high photostability unlike most organic dyes.[1−3] Owing to these unique optical properties, QDs were employed in light-emitting diodes (LEDs),[3−5] lasers,[6] photodetectors,[7] and solar cells.[8] Furthermore, their photophysical features have allowed for their use as donors and acceptors in nonradiative energy transfer (NRET).[9] These studies were reported for QDs in dispersion[10] and in solid film.[11,12] While working with films, QDs were frequently used in functional devices by incorporating them into polymer matrices (e.g., silicone). Another technique, recently reported by Otto et al.,[13] relies on the ionic crystal growth around colloidal QDs in salt solutions forming macrocrystals of these QDs. The attractive feature of this approach is its simplicity. The previously demonstrated crystalline host matrices[13−15] include NaCl, KCl, and KBr salts and sucrose,[16] which were shown to improve the robustness and stability of QDs. In all of these previous demonstrations of macrocrystals, QDs were integrated into water-soluble solutes. This has substantially limited the applicability of the QD macrocrystals because only those QDs that can be dispersed in water (aqueous QDs) could be used. For that purpose, QDs either had to be synthesized directly in water, which in the end limits the usable set of appropriate materials, or they had to undergo a phase transfer via ligand exchange, which typically reduces the quantum efficiency and may complicate the fabrication process. This creates a major limitation because most of the high-efficiency QDs are synthesized and dispersed in nonpolar solvents. Therefore, the use of a host crystal material that can be dissolved in organic solvents and is compatible with nonpolar QDs will remove this limiting requirement and widely broaden the applicability of the QD macrocrystals. As a candidate material system, in addition to their advantages such as low toxicity, abundance, and affordability, organic crystals that are composed of benzene group gain importance because they can be dissolved in organic solvents such as chloroform capable of dispersing nonpolar QDs.

Here we present the first account of organic crystal growth around nonpolar QDs using anthracene ($C_{14}H_{10}$) as the host crystal. In this work, we obtained large-scale QD-incorporated anthracene macrocrystals by using solvent evaporation technique. Structural characterization of anthracene with and without red-emitting CdSe/CdZnSeS/ZnS alloy QDs was carried out. It was found that the inclusion of these QDs in the anthracene solution allows for the growth of larger macrocrystals of over 1 cm in one dimension, which is otherwise limited to subcentimeter size (Figure 1a). Moreover,

**Received:** April 2, 2015
**Accepted:** April 23, 2015

  

DOI: 10.1021/acs.jpclett.5b00685
J. Phys. Chem. Lett. 2015, 6, 1767−1772

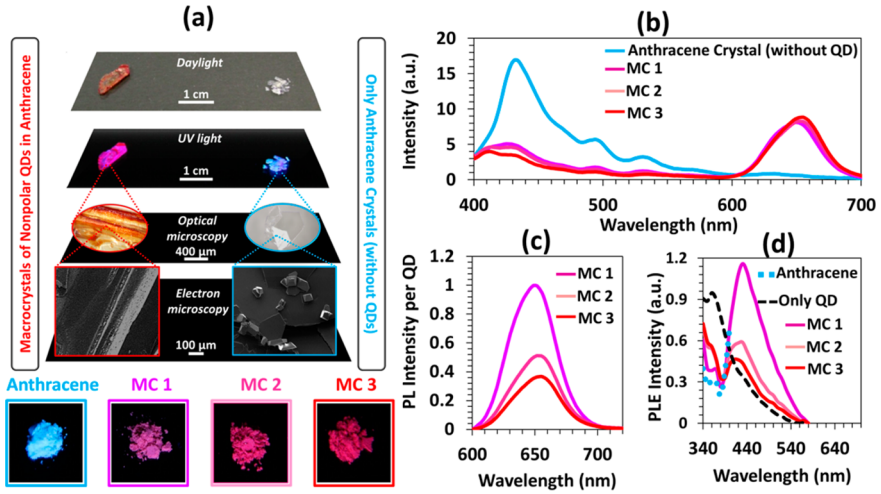


**Figure 1.** (a) Macroscopic images taken under ambient light and UV lamp illumination at 366 nm (scale bars: 1 cm). Imaging of the macrocrystal of nonpolar quantum dots in anthracene (left) and the anthracene crystals without quantum dots (right) performed by optical microscopy (scale bars: 400 $\mu$m) and scanning electron microscopy (scale bars: 100 $\mu$m) along with real color photographs of the powders belonging to the anthracene crystal, MC 1, MC 2, and MC 3 under UV lamp illumination at 366 nm. (b) Photoluminescence spectra of the films prepared using powders of the anthracene crystal alone (without QD incorporation) and MC 1, MC 2, and MC 3 (with QDs) when excited at 375 nm. (c) Normalized photoluminescence intensity per QD in MC 1, MC 2, and MC 3. (d) Photoluminescence excitation (PLE) spectra of MC 1, MC 2, and MC 3 normalized with respect to the QD amount along with that of the only QD film, all recorded in the emission wavelength range of 600−750 nm to collect the QD emission except the PLE of the anthracene crystal recorded between the emission wavelengths of 430 and 750 nm. A larger version of this Figure is also provided in Figure S6 in the SI.

we systematically studied NRET from the host anthracene acting as the donor to the inorganic QDs employed as the acceptor by benefiting from the strong absorption of QDs in the blue region where anthracene molecules emit strongly. Because anthracene has several photoluminescence (PL) peaks (at 429, 494, and 533 nm), we further investigated the NRET and lifetime decays at every peak as a function of the QD incorporation, and the maximum NRET efficiency was found to reach 28%. Developing an exciton transfer model, we studied the quantum efficiency of the anthracene emission contributing to each PL peak. We found that the most efficient anthracene emission occurs at the peak of 494 nm. In addition, the polarization of the QD emission inside the anthracene host was analyzed and found to reveal a vertical-to-parallel polarization ratio of ∼1.5 starting at 0° collection angle and increasing further to ∼2.5 at 60°. Finally, as a proof-of-concept demonstration, an LED was constructed by employing these QD-incorporated anthracene crystals as tunable color converters. This study reports for the first time the exciton transfer from the host organic crystal to the incorporated acceptor QDs together with its accompanying anisotropic emission and its application to tunable color-conversion LEDs. Because anthracene is especially important for electronics,[17] optoelectronics,[18−20] and physical chemistry,[17−21] this work may lead to new opportunities to utilize anthracene in these fields.

In this work, anthracene macrocrystals incorporating QDs were prepared using solvent evaporation method. Prior to our work, the growth and structure of anthracene crystals have been extensively studied.[21−23] Following the first report of anthracene crystals in 1948,[23] different crystal growth methodologies including the Bridgman−Stockbarger technique, physical vapor transfer method, and solution method were employed. Unlike the standard heat-assisted solution techniques,[22] here the solvent of the 1 mL anthracene solution (27.3 mg/mL) with and without the QDs was evaporated under laminar flow at room temperature. To systematically study the effect of the QDs on the physical and optical features of the macrocrystals, we grew macrocrystals using 6.5, 13.1, and 19.6 mg of QDs and named these samples MC 1, MC 2, and MC 3, respectively. We estimated the molar concentration of the QDs inside macrocrystals to be between 0.38 and 0.53 $\mu$mol/cm$^3$ for MC 1, between 0.81 and 1.12 $\mu$mol/cm$^3$ for MC 2, and between 1.44 and 1.74 $\mu$mol/cm$^3$. (See the Supporting Information (SI) for the details of this estimation.) After the formation of the final macrocrystals, microscopic and macroscopic structures of crystals were investigated using optical microscopy and SEM. It is apparent from Figure 1a that the resulting QD−anthracene macrocrystal (left) acquires a significantly larger size (centimeter scale) compared with the anthracene crystals alone without QD incorporation (subcentimeters) (right). Under ultraviolet illumination, the resulting emission color is red-violet in the case of QD−anthracene macrocrystal, while only anthracene crystals appear blue. As seen in Figure 1a, the crystal facets were obvious for the anthracene crystals. When QDs were embedded into the anthracene host, instead of clear crystal facets, we observed linear orientation of the crystal edges and the formation of relatively larger crystals. This suggests that QDs take role in the growth and orientation of anthracene in the crystallization process.

X-ray diffraction (XRD) analysis was also performed in powder form to investigate anthracene macrocrystals grown by incorporating varying amounts of QDs (Figure S1 in the SI). The crystal structure of anthracene was identified as monoclinic (JCPDS no. 04-0300). (001), (002), (003), (004), (005), and (006) crystal planes were observed in all anthracene crystals (Table S1 in the SI) being consistent with the previous reports.[24,25] The prominent peak corresponding to the (001) plane was observed at 9.44° ($d_{001}$ = 9.36 Å) for the anthracene alone. With the QD addition, the (001) and other equivalent peaks of all macrocrystals shifted toward larger angles. For instance, the diffraction peaks for the (001) plane were



DOI: 10.1021/acs.jpclett.5b00685
J. Phys. Chem. Lett. 2015, 6, 1767−1772

observed at 9.49 ($d_{001}$ = 9.31 Å), 9.51 ($d_{001}$ = 9.29 Å), and 9.55° ($d_{001}$ = 9.25 Å) for MC 1, MC 2, and MC 3, respectively (Figure S1 in the SI, inset). The decreasing pattern in the $d$ spacing suggests smaller lattice constants and increased strain within the macrocrystals owing to the QD incorporation. In addition, we observed an increase in the XRD signal between 24 and 28°, 41−47°, and 48−55° in the QD-embedded macrocrystals. In the report of Bae et al.,[26] zinc-blende QDs were shown to exhibit XRD peaks at 27.5, 46.0, and 55.0°. Consistent with these XRD peaks, here we associate the XRD signals at the observed angles to the QDs incorporated into the anthracene host.

We started the optical characterization by taking the PL spectra of the anthracene crystals and the QD−anthracene macrocrystals. As shown in Figure 1b, the anthracene crystals exhibit PL peaks at the wavelengths of 429, 494, and 533 nm when excited at 375 nm. In the case of the QD−anthracene macrocrystals, we also observe another peak around 653 nm owing to the emission from the incorporated QDs. With the increasing incorporation amount of the QDs, we observe a slight red shift in the emission peak of the QDs, suggesting possible formation of some aggregates inside the macrocrystals. In addition, we observed a strong decrease in the emission of the anthracene host accompanied by an increase in the emission intensity per QD (Figure 1c). While the radiative energy transfer plays a role for this decrease in the steady-state emission intensity of the anthracene, it does not modify emission kinetics. Therefore, to investigate the NRET, we analyzed the time-resolved fluorescence decays of the QDs inside the macrocrystals. Our results presented in Figure 2a and

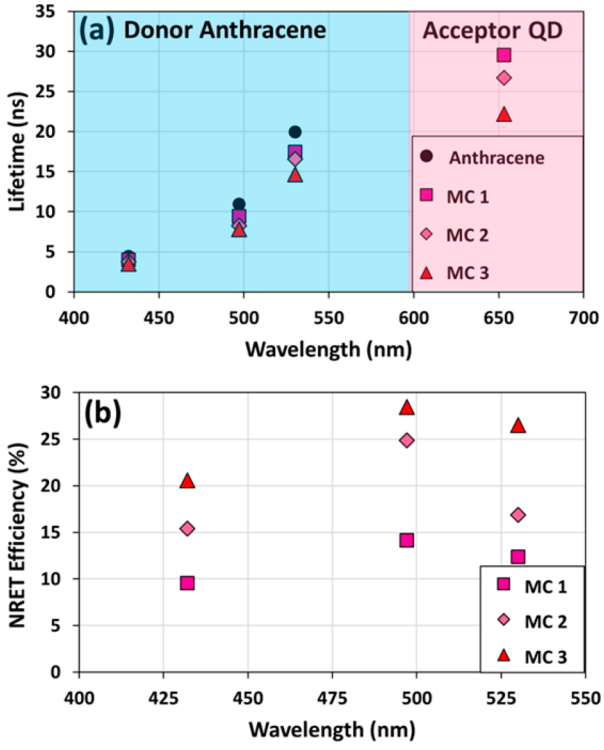


**Figure 2.** (a) Photoluminescence decay lifetimes of the anthracene emission at 429, 494, and 533 nm in the anthracene crystals and anthracene−QD macrocrystals (MC 1, MC 2, and MC 3) together with the lifetimes of the QD emission at 653 nm. All of the samples are excited at 375 nm. (b) Nonradiative energy transfer (NRET) efficiencies at the wavelengths where the donor lifetimes are measured.

Figures S2−S4 and Table S2 in the SI show that the anthracene PL decay accelerates in the presence of QDs. Furthermore, the anthracene fluorescence lifetimes become shorter with the increasing QD incorporation. The presented results indicate longer lifetimes of the QDs in anthracene with the increasing anthracene-to-QD mass ratio accompanied by an increased delay of the QD decay curve (Figure S5 in the SI). Complementary to the decrease in anthracene emission and increase in the emission intensity per QD, these lifetime modifications suggest that the Förster-like NRET takes place from the host anthracene molecules to the embedded QDs.[27,28] Additionally, we do not observe any fast decay component in the time-resolved fluorescence decay of the QDs, suggesting that there is no significant fast charge transfer,[27] which is prevented by the ZnS shell coating of the QDs.[28] Moreover, the photoluminescence excitation (PLE) spectra of the QDs in the macrocrystals significantly differ from those of the only QDs and mimic the PLE spectrum of anthracene crystal in its absorption range (Figures 1d and Figure S6 in the SI). However, toward shorter wavelengths where the anthracene does not absorb light, the QD emission in the macrocrystals tends to follow the trend of the only QD film. This shows that the excitation of anthracene molecules strongly triggers the emission of the QDs in the macrocrystals. Considering all of these arguments, here we conclude that Förster-like NRET is the most dominant NRET mechanism in our macrocrystal system.

To analyze the energy-transfer mechanism inside the macrocrystals, we systematically recorded the time-resolved fluorescence decay lifetimes at each PL peak of the exciton donating anthracene molecules as a function of the incorporated QD amount. We calculated the NRET efficiency ($\eta$) from the donor lifetime modification using the Förster theory employing eq 1, where $\tau_D$ and $\tau_{DA}$ stand for the amplitude averaged lifetimes of the donor in the absence and presence of acceptor, respectively.

$$\eta = \frac{1/\tau_{DA} - 1/\tau_D}{1/\tau_{DA}} \quad (1)$$

At 429 nm, we observe accelerated time-resolved fluorescence decays as a result of the NRET from the anthracene host to the acceptor QDs. Corresponding lifetimes decrease from 4.45 to 4.02, 3.76, and 3.53 ns for MC 1, MC 2, and MC 3, respectively (Figure S2 in the SI, Figure 2a, and Table S2 in the SI). Consequently, the NRET efficiencies turn out to be 9.6, 15.4, and 20.6% for MC 1, MC 2, and MC 3, respectively (Figure 2b and Table S3 in the SI). At 494 nm, we observe a similar acceleration pattern in the PL decays as in the case of 429 nm. The lifetime of the anthracene emission decreases from 11.0 to 9.42, 8.24, and 7.84 ns for MC 1, MC 2, and MC 3, respectively (Figure S3 in the SI, Figure 2a, and Table S2 in the SI). These lifetimes indicate a more efficient exciton-transfer process compared with that at 429 nm with $\eta$ reaching 14.1, 24.9, and 28.5%, respectively (Figure 2b and Table S3 in the SI). At 533 nm, the variation of the lifetimes and NRET efficiencies follow the same pattern as the amount of QD incorporation increases. While the emission decay lifetime of the anthracene crystals without QD incorporation is 19.9 ns, the incorporation of QD decreases this value within macrocrystals to 17.5, 16.6, and 14.7 ns for MC 1, MC 2, and MC 3 (Figure S4 in the SI, Figure 2a, and Table S2 in the SI), respectively, corresponding to 12.4, 16.9, and 26.5% NRET


DOI: 10.1021/acs.jpclett.5b00685
J. Phys. Chem. Lett. 2015, 6, 1767−1772

efficiencies (Figure 2b and Table S3 in the SI). The rates of the NRET presented in Table S3 in the SI follow the same increasing pattern as the QD amount increases. We attribute this decrease in the donor lifetimes (and increase in NRET rates) to the increased NRET from the anthracene molecules to QDs going from MC1 to MC3. This is because there are more acceptor QDs available per donor anthracene molecule to feed excitons going from sample MC 1 to MC 3. Therefore, a donor anthracene molecule should transfer more excitons going from MC 1 to MC 3. This then results in shorter anthracene lifetimes going from MC 1 to MC 3. In a complementary manner, there are fewer anthracene molecules per acceptor QD going from MC 1 to MC 3. Therefore, a QD has fewer excitons transferred to it going from MC 1 to MC 3; consequently, the QD lifetime decreases as going from MC 1 to MC 3 (Figure S5 and Table S2 in the SI). This observation is further supported by the shorter delays of the acceptor decay curves, decreasing PLE intensity per QD (Figures 1d and Figure S6 in the SI), and decreasing PL intensities per QD (Figure 1c) going from MC 1 to MC 3.

In our experiments, we observe that the acceptor lifetime shortens from 29.5 ns in MC 1, to 26.7 ns in MC 2, and 22.2 ns in MC 3 with increasing QD concentration in macrocrystals. These results are in parallel with the study of Mutlugun et al.,[29] where acceptor lifetimes shortened with increasing acceptor concentration; however, they always remained longer than the acceptor lifetime in the absence of donor. Our results are also consistent with the theoretical acceptor decay model of Lindhoud et al.[30] showing that the acceptor lifetime shortens as the acceptor-to-donor concentration ratio increases. This model also predicts that the acceptor lifetime in the presence of donor always remains longer than that in the absence of donor (Figure S7 in the SI). In our experiments, we cannot present the acceptor lifetime in the absence of donor because the host itself acts as the donor and choosing any other host material would change the photophysical characteristics of the incorporated QDs; however, to have an idea about the acceptor lifetime without a donor, we measured the lifetime of drop-casted QDs to be 4.90 ns, which is much shorter than the lifetime of the QDs in anthracene macrocrystals. In addition to this, we estimated the acceptor lifetime in the absence of donor using the model in ref 30 to be around 9.2−13.0 ns, which is also shorter than the acceptor lifetime in the presence of acceptor.

To gain further insight into the physical mechanisms behind, we predicted the surface-to-surface distance to be between QDs between 8.4 and 9.9 nm for MC 1, between 4.9 and 6.2 nm for MC 2, and between 3.4 and 4.0 nm for MC 3, which are shorter than the predicted Förster radii. (See the SI for details.) These results indicate strengthened sharing of excitons with the increasing QD concentration. As a consequence, increasing the QD concentration decreases the number of excitons received by each QD, leading to shorter acceptor lifetimes; however, these transferred excitons to QDs still make the acceptor lifetimes in the macrocrystals longer compared with the case of without donor.

To reveal the physical reasoning behind the observation that the NRET at longer wavelengths occurs more efficiently compared with 429 nm, we investigated the relation between the overlap integral ($J$) and the quantum yield at the wavelength of interest ($Q(\lambda)$) by assuming the random distribution of exciton-donating anthracene molecules and the acceptor QDs. The details of our semiempirical model are presented in the SI. Our results summarized in Figure S9 in the SI show that the overlap integral remains unaffected although the absorption of the QDs is stronger at shorter wavelengths. This is mainly because of the fourth power dependence of the overlap integral on the wavelength. Subsequently, we calculated the normalized Förster radius ($R_0^6$) (Figure S10a in the SI) and then calculated normalized quantum efficiency (Figure S10b in the SI). Here we observe that the quantum efficiency takes its highest value for all the at 494 nm, where the NRET occurs most efficiently. Considering the wavelength dependence of the overlap integral and quantum efficiency, we conclude that the difference of the NRET efficiency is essentially caused by the difference in the quantum efficiency at each wavelength, reaching its highest value at 494 nm.

Because the optical properties of the anthracene are anisotropic,[31,32] their macrocrystals might be expected to enhance the emission anisotropy of the incorporated QDs. To examine this hypothesis, we systematically investigated the polarization of the emitted light from the QDs that are immobilized in single anthracene−QD macrocrystals (not in powdered form). Here we employed a single centimeter-scale macrocrystal taken from the batch of MC 3 because of its larger size, making the optical anisotropy measurements easier. Our results show that when the photons emitted normal to the surface of the anthracene−QD macrocrystal are collected, the ratio of the perpendicular polarization to the parallel polarization was measured to be ∼1.50 (Figure 3 and Figure S11a in the SI). Increasing the collection angle to 30°, no significant change in the anisotropy of the QD emission was observed (Figure 3 and Figure S11b in the SI). A further increase in the collection angle to 60° improved the polarization ratio to ∼2.50 (Figure 3 and Figure S11c in the SI). This observed anisotropy in the QD emission can either stem from the anisotropic extraction of electromagnetic radiation at different polarizations or from the emission rate difference caused by the anisotropy in the refractive index of the medium. One of the important indicators of the latter mechanism is the difference of the PL decay lifetimes at different polarizations. To identify the governing effect in our system, we investigated the emission dynamics of the QDs for both of the polarizations and did not measure a noticeable difference in the lifetime, which suggests that the main source of the observed anisotropy is the extraction efficiency difference rather than the modification of spontaneous emission rate.

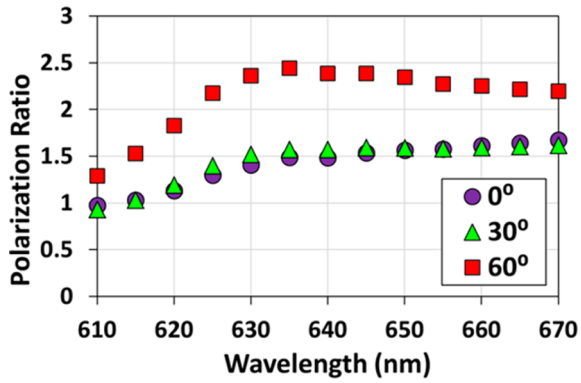


**Figure 3.** Ratio of polarizations of the QD emission within MC 3 at different collection angles.



DOI: 10.1021/acs.jpclett.5b00685
J. Phys. Chem. Lett. 2015, 6, 1767−1772

Finally, we present a proof-of-concept demonstration of these anthracene−QD macrocrystals as color-enrichment films on a commercially available LED emitting at 380 nm. The photons emitted from the LED at this wavelength were strongly absorbed by both the anthracene molecules and the QDs in the macrocrystal. As a result of the PL of the anthracene and QDs and the NRET between them, the color conversion results in the emission spectra in Figure 4 for MC 3 LED (and Figure S12a−c in the SI for MC 1, MC 2, and MC 3 LEDs) and the corresponding color coordinates presented in Figure S12d in the SI. The results show a trend in the change of the obtained color as the incorporated QD amount varies, as expected, due to the both radiative and NRET. This proof-of-concept demonstration indicates that the anthracene crystal is a good host for the QDs to be integrated into color conversion LEDs thanks to its compatibility with the transparent epoxies used by the industry.

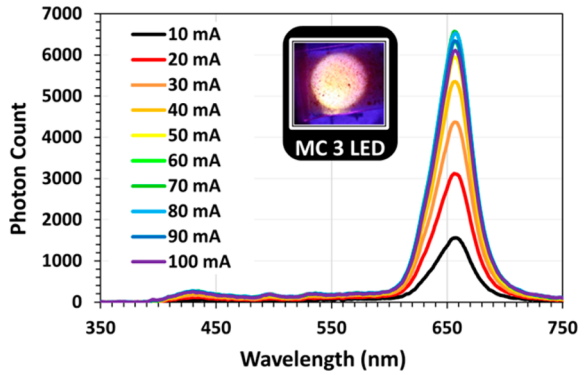


**Figure 4.** Emission spectra belonging to the color-converting powdered film of MC 3 on a UV LED emitting at 380 nm driven by 10−100 mA along with its real color photograph.

In summary, here we demonstrated anthracene−QD macrocrystals to elucidate the interaction of the QDs within the host anthracene crystals. First, we carried out structural characterizations using optical and scanning electron microscopies. We observed that the QD incorporation affects the crystallization process of anthracene and leads to the formation of larger macrocrystals. Subsequently, we investigated the NRET dynamics where the anthracene and the QDs serve as the exciton donating and accepting entities in the macrocrystal, respectively. Our results showed that the PL lifetime of the anthracene molecules decreases with the increasing QD incorporation, indicating stronger exciton transfer. Moreover, we found that the anthracene does not emit most efficiently at the main PL peak at 429 nm in the presence of the QDs inside the macrocrystals, but instead the highest quantum efficiency occurs at 494 nm. In addition to this, the polarization anisotropy of the QD emission was observed at various collection angles. We found that these QDs exhibit a ∼1.5 polarization ratio at the surface normal collection, while this number increases to ∼2.5 at the collection angle of 60°. Finally, we used this NRET concept on a color-conversion LED employing the anthracene−QD macrocrystal as the color conversion film and demonstrated color tunability as a function of the incorporated QD amount. We believe that the findings of this study may open up new possibilities for employing crystalline organic semiconductors such as anthracene in the field of colloidal photonics.

## EXPERIMENTAL SECTION

Details of the colloidal QD synthesis, calculation of the QD to anthracene weight ratio in the macrocrystals, film preparation and LED fabrication, and optical and structural characterizations are presented in the SI.

*Preparation of Anthracene Crystals and Anthracene−QD Macrocrystals.* Macrocrystals were obtained by crystallization of oversaturated anthracene solution in chloroform. To prepare oversaturated anthracene stock solution, we dissolved 2.08 g of anthracene in 50 mL of chloroform. After the filtration using a filter with a pore size of 0.2 $\mu$m, the concentration of the anthracene stock solution was measured to be 27.3 mg/mL. To grow anthracene crystals, 1 mL of this stock solution was dried in a vial in a laminar flow hood at room temperature. The anthracene−QD macrocrystals were formed by mixing the QD solution and anthracene stock solution. For the systematic study, 6.5, 13.1, and 19.6 mg of red-emitting QDs were used, and these samples were named MC 1, MC 2, and MC 3, respectively. To obtain macrocrystals, we added 250 $\mu$L of chloroform to the desired concentrations of QDs (MC 1, MC2, and MC 3) after the evaporation of hexane, and the dispersion was mixed with 1 mL of anthracene stock solution. Chloroform was evaporated under laminar flow for 2 days to obtain macrocrystals.

## ASSOCIATED CONTENT

### Supporting Information

Details of colloidal QD synthesis, calculation of the QD to anthracene weight ratio in the macrocrystals, film preparation and LED fabrication, and optical and structural characterizations. Figures of X-ray powder diffraction pattern of macrocrystals, time-resolved fluorescence lifetime decays of macrocrystals, PLE spectra of the macrocrystals, ratio of the acceptor lifetime in the presence and absence of donor, emission spectrum and multiple Gaussian function fit of anthracene macrocrystals, the overlap integral between QD absorption and individual emission mechanism, normalized Förster radius and relative quantum efficiency of the anthracene emission, emission spectra of the QDs in the macrocrystals at different polarizations, and emission spectra and chromaticity points of the LEDs. Tables of XRD peak locations, time-resolved fluorescence decay lifetimes, and NRET efficiencies and rates. Calculation methodology of molar concentration of QDs and spacing between QDs in macrocrystals. Details of semiempirical model for NRET. The Supporting Information is available free of charge on the ACS Publications website at DOI: 10.1021/acs.jpclett.5b00685.

## AUTHOR INFORMATION

### Corresponding Author

*E-mail: volkan@stanfordalumni.org. Phone: [+90] (312) 290-1021. Fax: [+90] (312) 290-1123.

### Author Contributions

‖Z.S.-E. and T.E. contributed equally to this work.

### Notes

The authors declare no competing financial interest.

## ACKNOWLEDGMENTS

We acknowledge ESF EURYI, EU-FP7 Nanophotonics4Energy NoE, BMBF TUR 09/001, and TUBITAK EEEAG 109E002, 109E004, 110E010, 110E217, 112E183 and partial support by NRF-CRP-6-2010-02 and NRF-RF-2009-09. H.V.D. acknowl-



DOI: 10.1021/acs.jpclett.5b00685
J. Phys. Chem. Lett. 2015, 6, 1767−1772

edges additional support from TUBA-GEBIP and T.E. acknowledges support from TUBITAK BIDEB.

## REFERENCES

(1) Demir, H. V.; Nizamoglu, S.; Erdem, T.; Mutlugun, E.; Gaponik, N.; Eychmüller, A. Quantum Dot Integrated LEDs Using Photonic and Excitonic Color Conversion. *Nano Today* **2011**, *6*, 632−647.
(2) Kim, J. Y.; Voznyy, O.; Zhitomirsky, D.; Sargent, E. H. 25th Anniversary Article: Colloidal Quantum Dot Materials and Devices: A Quarter-Century of Advances. *Adv. Mater.* **2013**, *25*, 4986−5010.
(3) Shirasaki, Y.; Supran, G. J.; Bawendi, M. G.; Bulović, V. Emergence of Colloidal Quantum-Dot Light-Emitting Technologies. *Nat. Photonics* **2013**, *7*, 13−23.
(4) Erdem, T.; Demir, H. V. Color Science of Nanocrystal Quantum Dots for Lighting and Displays. *Nanophotonics* **2013**, *2*, 57−81.
(5) Mutlugun, E.; Guzelturk, B.; Abiyasa, A. P.; Gao, Y.; Sun, X. W.; Demir, H. V. Colloidal Quantum Dot Light-Emitting Diodes Employing Phosphorescent Small Organic Molecules as Efficient Exciton Harvesters. *J. Phys. Chem. Lett.* **2014**, *5*, 2802−2807.
(6) Guzelturk, B.; Kelestemur, Y.; Akgul, M. Z.; Sharma, V. K.; Demir, H. V. Ultralow Threshold One-Photon and Two-Photon Pumped Optical Gain Media of Blue-Emitting Colloidal Quantum Dot Films. *J. Phys. Chem. Lett.* **2014**, *5*, 2214−2218.
(7) Sukhovatkin, V.; Hinds, S.; Brzozowski, L.; Sargent, E. H. Colloidal Quantum-dot Photodetectors Exploiting Multiexciton Generation. *Science* **2009**, *324*, 1542−1544.
(8) Kamat, P. V. Quantum Dot Solar Cells. Semiconductor Nanocrystals as Light Harvesters. *J. Phys. Chem. C* **2008**, *112*, 18737−18753.
(9) Guzelturk, B.; Hernandez-Martinez, P. L.; Zhang, Q.; Xiong, Q.; Sun, H.; Sun, X. W.; Govorov, A. O.; Demir, H. V. Excitonics of Semiconductor Quantum Dots and Wires for Lighting and Displays. *Laser Photonics Rev.* **2014**, *8*, 73−93.
(10) Mutlugun, E.; Nizamoglu, S.; Demir, H. V. Highly Efficient Nonradiative Energy Transfer Using Charged CdSe/ZnS Nanocrystals for Light-harvesting in Solution. *Appl. Phys. Lett.* **2009**, *95*, 033106.
(11) Yeltik, A.; Guzelturk, B.; Hernandez-Martinez, P. L.; Govorov, A. O.; Demir, H. V. Phonon-Assisted Exciton Transfer into Silicon Using Nanoemitters: The Role of Phonons and Temperature Effects in Förster Resonance Energy Transfer. *ACS Nano* **2013**, *7*, 10492−10501.
(12) Cicek, N.; Nizamoglu, S.; Ozel, T.; Mutlugun, E.; Karatay, D. U.; Lesnyak, V.; Otto, T.; Gaponik, N.; Eychmüller, A.; Demir, H. V. Structural Tuning of Color Chromaticity Through Nonradiative Energy Transfer by Interspacing CdTe Nanocrystal Monolayers. *Appl. Phys. Lett.* **2009**, *94*, 061105.
(13) Otto, T.; Müller, M.; Mundra, P.; Lesnyak, V.; Demir, H. V.; Gaponik, N.; Eychmüller, A. Colloidal Nanocrystals Embedded in Macrocrystals: Robustness, Photostability, and Color Purity. *Nano Lett.* **2012**, *12*, 5348−5354.
(14) Müller, M.; Kaiser, M.; Stachowski, G.; Resch-Genger, U.; Gaponik, N.; Eychmüller, A. Photoluminescence Quantum Yield and Matrix-induced Luminescence Enhancement of Colloidal Quantum Dots Embedded in Ionic Crystals. *Chem. Mater.* **2014**, *26*, 3231−3237.
(15) Kalytchuk, S.; Zhovtiuk, O.; Rogach, A. L. Sodium Chloride Protected CdTe Quantum Dot Based Solid-state Luminophores with High Color Quality and Fluorescence Efficiency. *Appl. Phys. Lett.* **2013**, *103*, 103105.
(16) Erdem, T.; Soran-Erdem, Z.; Hernandez-Martinez, P. L.; Sharma, V. K.; Akcali, H.; Akcali, I.; Gaponik, N.; Eychmüller, A.; Demir, H. V. Sweet Plasmonics: Sucrose Macrocrystals of Metal Nanoparticles. *Nano Res.* **2015**, *8*, 860−869.
(17) Briseno, A. L.; Mannsfeld, S. C.; Ling, M. M.; Liu, S.; Tseng, R. J.; Reese, C.; Roberts, M. E.; Yang, Y.; Wudl, F.; Bao, Z. Patterning Organic Single-crystal Transistor Arrays. *Nature* **2006**, *444*, 913−917.
(18) Raghunath, P.; Reddy, M. A.; Gouri, C.; Bhanuprakash, K.; Rao, V. J. Electronic Properties of Anthracene Derivatives for Blue Light Emitting Electroluminescent Layers in Organic Light Emitting Diodes: A Density Functional Theory Study. *J. Phys. Chem. A* **2006**, *26*, 1152−1162.
(19) Tao, S.; Zhou, Y.; Lee, C.-S.; Lee, S.-T.; Huang, D.; Zhang, X. Highly Efficient Nondoped Blue Organic Light-emitting Diodes Based on Anthracene-triphenylamine Derivatives. *J. Phys. Chem. C* **2008**, *112*, 14603−14606.
(20) Benmansour, H.; Shioya, T.; Sato, Y.; Bazan, G. C. Anthracene-Containing Binaphthol Chromophores for Light-emitting Diode (LED) Fabrication. *Adv. Funct. Mater.* **2003**, *13*, 883−886.
(21) Briseno, A. L.; Aizenberg, J.; Han, Y.-J.; Penkala, R. A.; Moon, H.; Lovinger, A. J.; Kloc, C.; Bao, Z. Patterned Growth of Large Oriented Organic Semiconductor Single Crystals on Self-assembled Monolayer Templates. *J. Am. Chem. Soc.* **2005**, *127*, 12164−12165.
(22) Lipsett, F. On the Production of Single Crystals of Naphthalene and Anthracene. *Can. J. Phys.* **1957**, *35*, 284−298.
(23) Feazel, C. E.; Smith, C. D. Production of Large Crystals of Naphthalene and Anthracene. *Rev. Sci. Instrum.* **1948**, *19*, 817−818.
(24) Jo, S.; Yoshikawa, H.; Fujii, A. Surface Morphologies of Anthracene Single Crystals Grown from Vapor Phase. *Appl. Surf. Sci.* **2006**, *252*, 3514−3519.
(25) Wu, H.; Zhou, J. Optical Properties of Anthracene Single Crystals Grown by a Simple Solution Technique. *Int. J. Mod. Phys. B* **2013**, *27*, 1350022.
(26) Bae, W. K.; Char, K.; Hur, H.; Lee, S. Single-step Synthesis of Quantum Dots with Chemical Composition Gradients. *Chem. Mater.* **2008**, *20*, 531−539.
(27) Koeppe, R.; Sarıçiftçi, N. S. Photoinduced Charge and Energy Transfer Involving Fullerene Derivatives. *Photobiol. Sci.* **2006**, *5*, 1122−1131.
(28) Nizamoglu, S.; Sari, E.; Baek, J.-H.; Lee, I.-H.; Demir, H. V. Nonradiative Resonance Energy Transfer Directed from Colloidal CdSe/ZnS Quantum Dots to Epitaxial InGaN/GaN Quantum Wells for Solar Cells. *Phys. Status Solidi RRL* **2010**, *4*, 178−180.
(29) Mutlugun, E.; Samarskaya, O.; Ozel, T.; Cicek, N.; Gaponik, N.; Eychmüller, A.; Demir, H. V. Highly Efficient Nonradiative Energy Transfer Mediated Light Harvesting in Water Using Aqueous CdTe Quantum Dot Antennas. *Opt. Express* **2010**, *18*, 10720−10730.
(30) Lindhoud, S.; Westphal, A. H.; van Mierlo, C. P. M.; Visser, A. J. W. G.; Borst, J. W. Rise-Time of FRET-Acceptor Fluorescence Tracks Protein Folding. *Int. J. Mol. Sci.* **2014**, *15*, 23836−23850.
(31) Nakada, I. The Optical Properties of Anthracene Single Crystals. *J. Phys. Soc. Jpn.* **1962**, *17*, 113−118.
(32) Lasheen, M.; Abdeen, A. Optical Anisotropies of Some Organic Molecules. *Acta Crystallogr., Sect. A* **1972**, *28*, 245−249.



DOI: 10.1021/acs.jpclett.5b00685
*J. Phys. Chem. Lett.* 2015, 6, 1767−1772